Supporting Information for

Ligand Triplet Energy Escape in Lanthanide Complexes for Developing Luminescent Molecular Thermometers

Yusaku Yamaguchi[1], Takuma Nakai[1], Shun Omagari[2], Mengfei Wang[3,4], Yasuchika Hasegawa[3,4] Yuichi Kitagawa[3,4]

[1]*Graduate School of Chemical Sciences and Engineering, Hokkaido University, Kita 13, Nishi 8, Kita-ku, Sapporo, Hokkaido 060-8628, Japan*

[2]*Department of Materials Science and Engineering, Institute of Science Tokyo, Ookayama 2-12-1, Meguro-ku, Tokyo 152-8552, Japan*

[3]*Institute for Chemical Reaction Design and Discovery (WPI-ICReDD), Hokkaido University, Kita 21, Nishi 10, Kita-ku, Sapporo, Hokkaido 001-0021, Japan*

[4]*Faculty of Engineering, Hokkaido University, Kita 13, Nishi 8, Kita-ku, Sapporo, Hokkaido 060-8628, Japan*

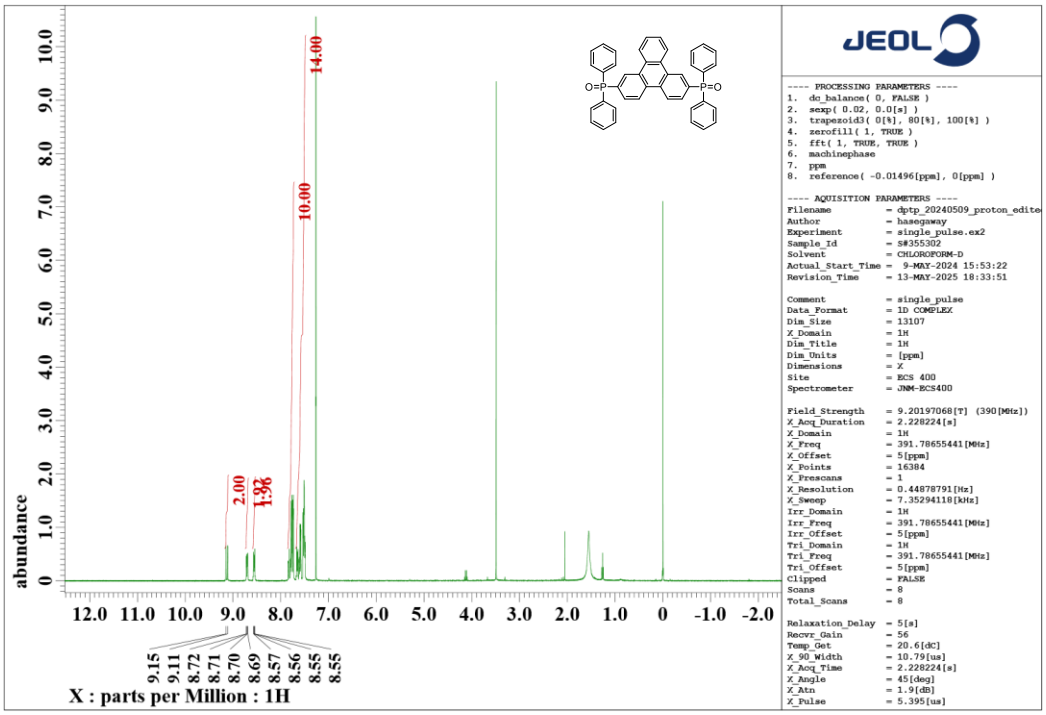

Supplementary Fig. 1 ^{1}H-NMR spectrum of dptp in $CDCl_3$.

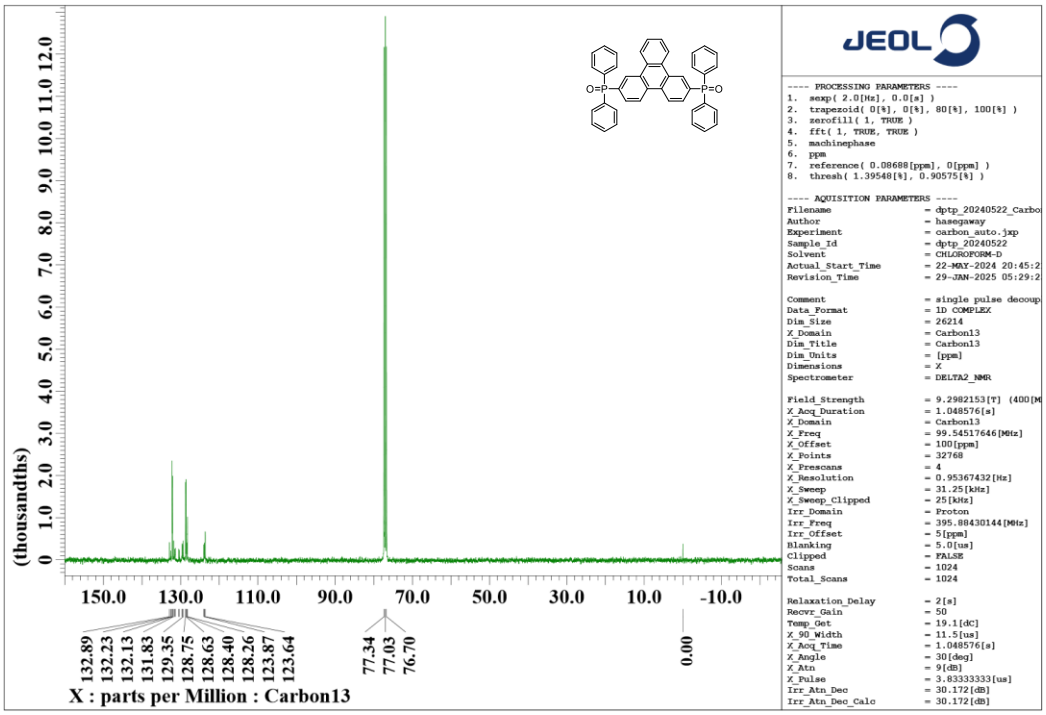

Supplementary Fig. 2 ^{13}C-NMR spectrum of dptp in $CDCl_3$.

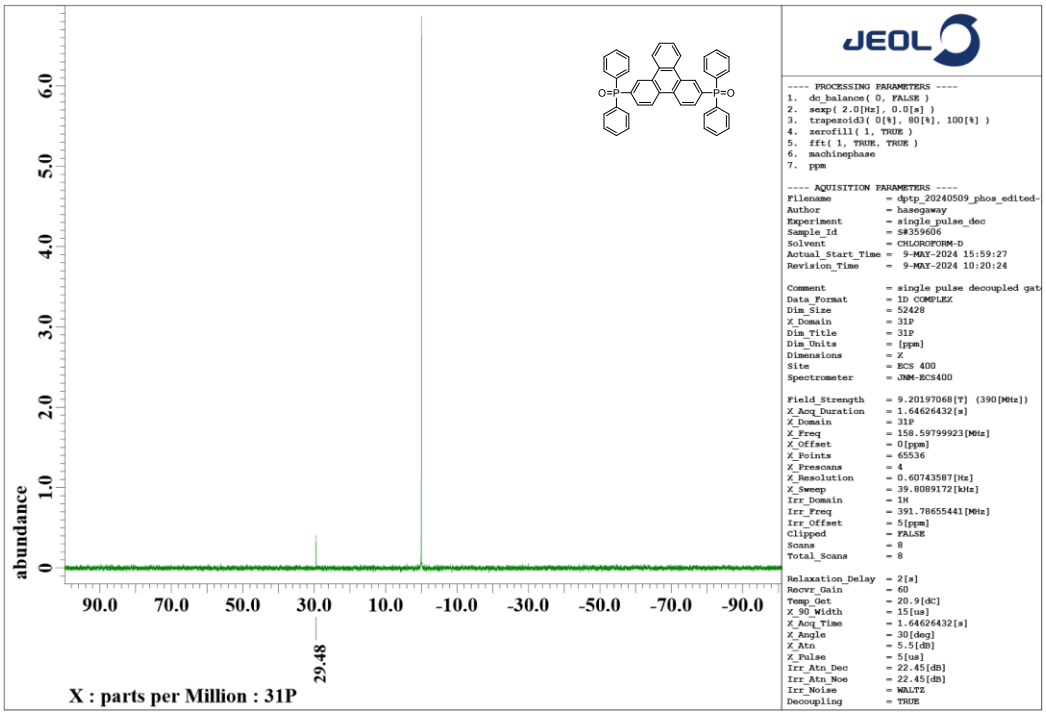

Supplementary Fig. 3 ^{31}P-NMR spectrum of dptp in $CDCl_3$.

Supplementary Table 1 Crystallographic data for $[Tb_2(hfa)_6(dptp)_2]$.

	$[Tb_2(hfa)_6(dptp)_2]$
Chemical formula	$C_{114}H_{66}F_{36}O_{16}P_4Tb_2$
Crystal system	Orthorhombic
Space group	*Pccn*
a / Å	40.9140(15)
b / Å	31.3064(15)
c / Å	18.6551(5)
Volume / Å^3	23894.8(16)
Z	8
Density / g cm^{-3}	1.566
Temperature / ℃	−150
R	0.0667
wR_2	0.1508

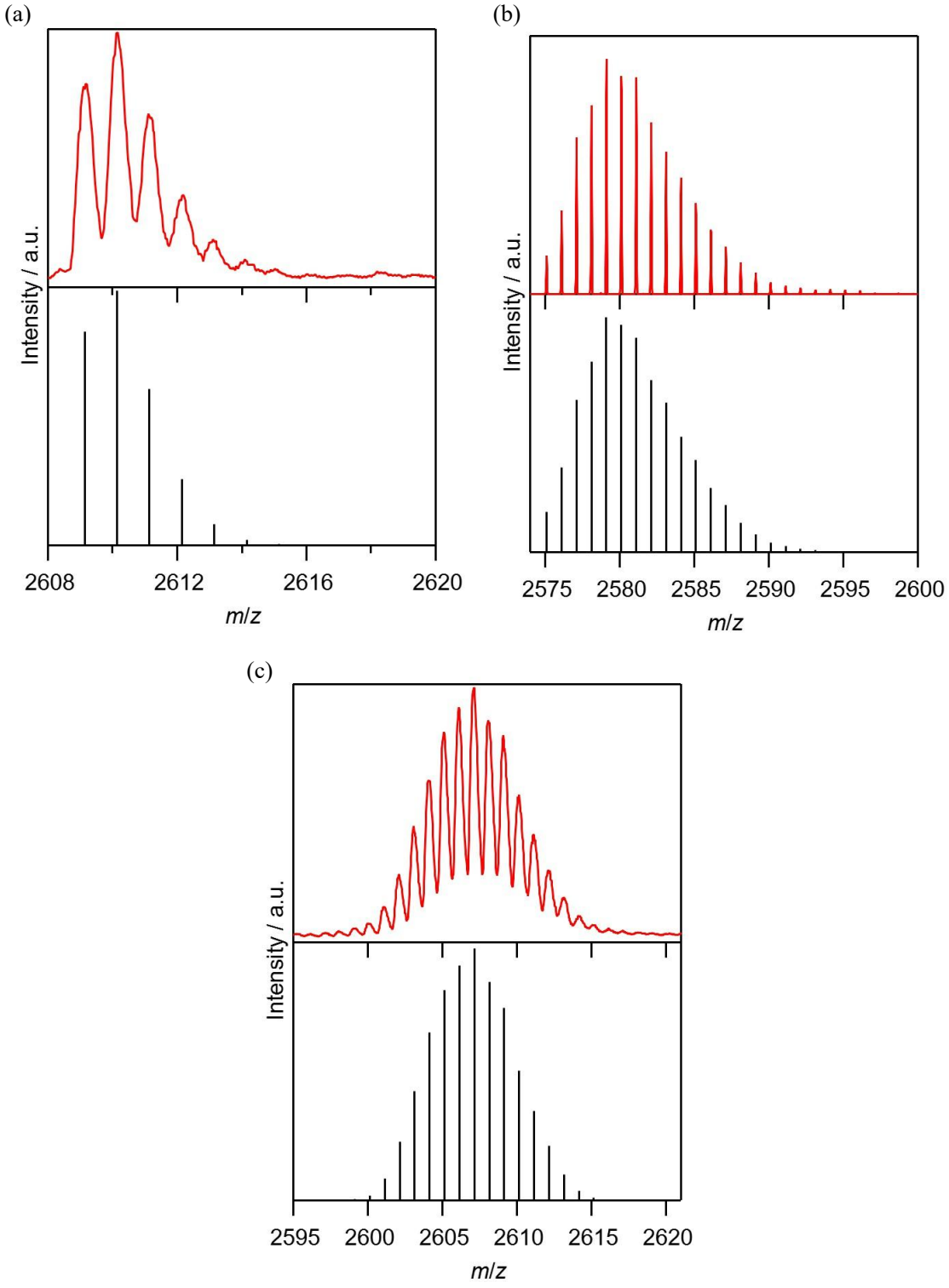

Supplementary Fig. 4 Experimental ESI-MS spectra of (a) $[Tb_2(hfa)_6(dptp)_2]$, (b) $[Nd_2(hfa)_6(dptp)_2]$, and (c) $[Gd_2(hfa)_6(dptp)_2]$ (red lines). Calculated ESI-MS spectra of (a) $[Tb_2(hfa)_5(dptp)_2]^+$, (b) $[Nd_2(hfa)_5(dptp)_2]^+$, and (c) $[Gd_2(hfa)_5(dptp)_2]^+$ (black lines).

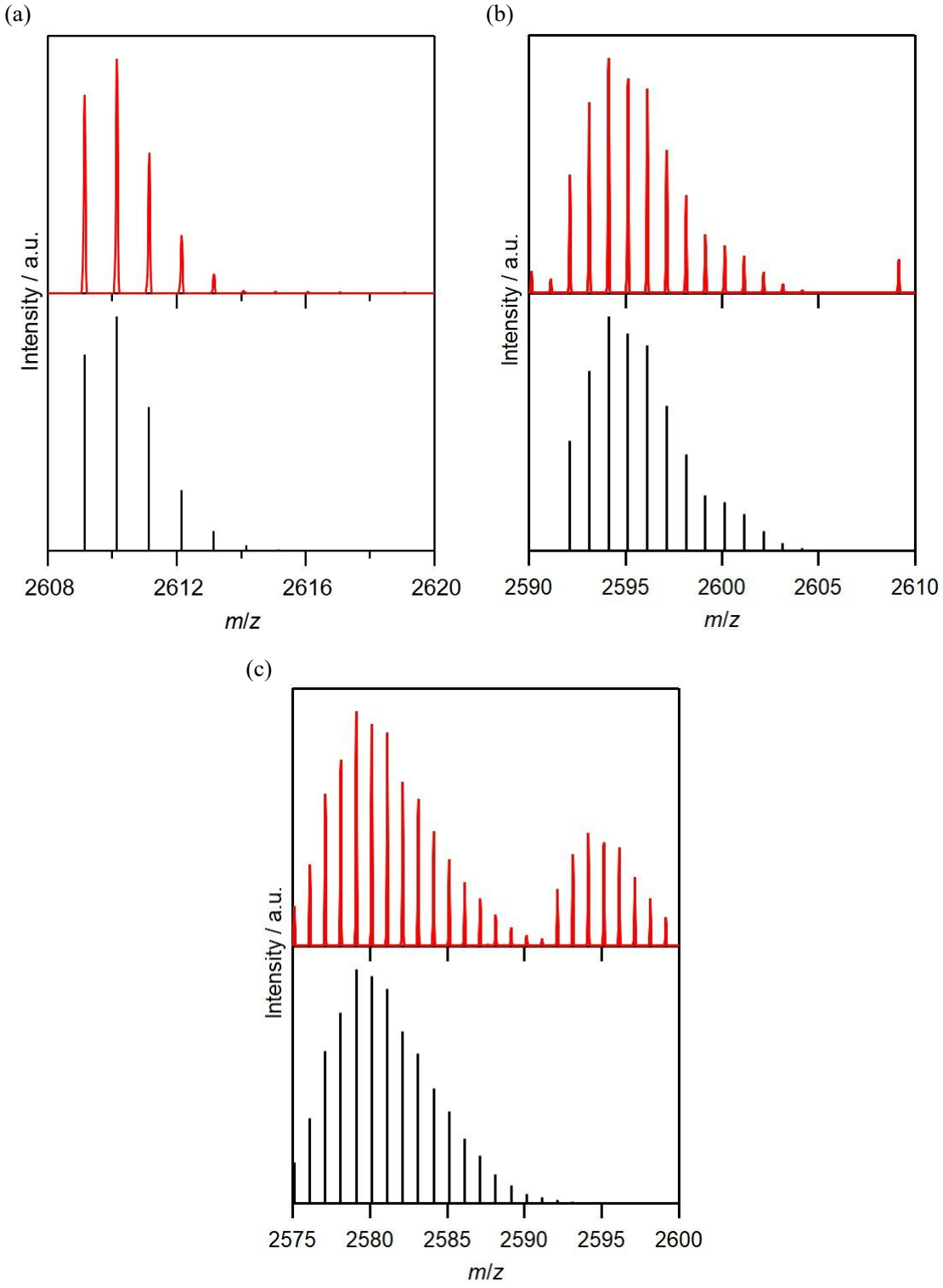

Supplementary Fig. 5 Experimental ESI-MS spectra of Tb-Nd mixed crystal (a-c, red lines). Calculated ESI-MS spectra of (a) $[Tb_2(hfa)_5(dptp)_2]^+$, (b) $[TbNd(hfa)_5(dptp)_2]^+$, and (c) $[Nd_2(hfa)_5(dptp)_2]^+$ (black lines).

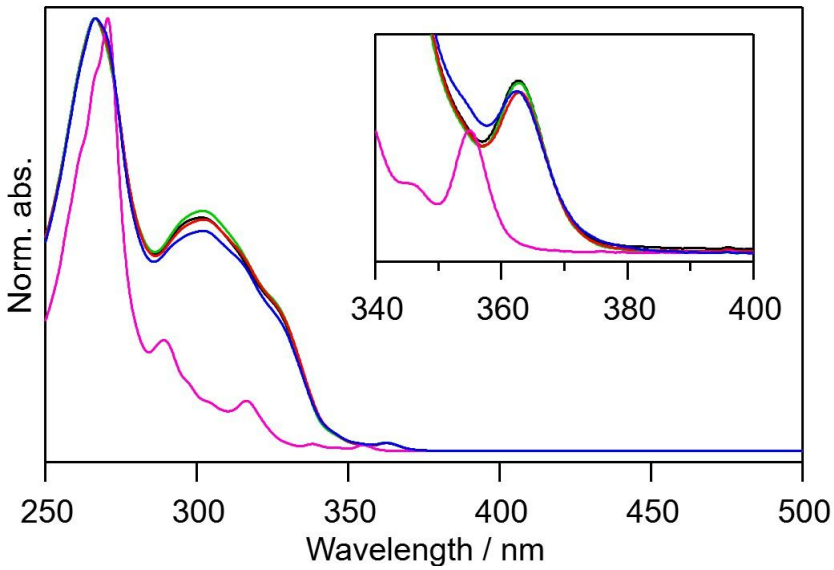

Supplementary Fig. 6 Electronic absorption spectra of $[Tb_2(hfa)_6(dptp)_2]$ (0.1 mM, black line), $[Nd_2(hfa)_6(dptp)_2]$ (0.1 mM, blue line), $[Gd_2(hfa)_6(dptp)_2]$ (0.1 mM, green line), and dptp ligand (0.2 mM, pink line) dissolved in 2-MeTHF and Tb-Nd_{MeTHF} (0.1 mM, red line). The spectra are normalized at their maximum absorbance.

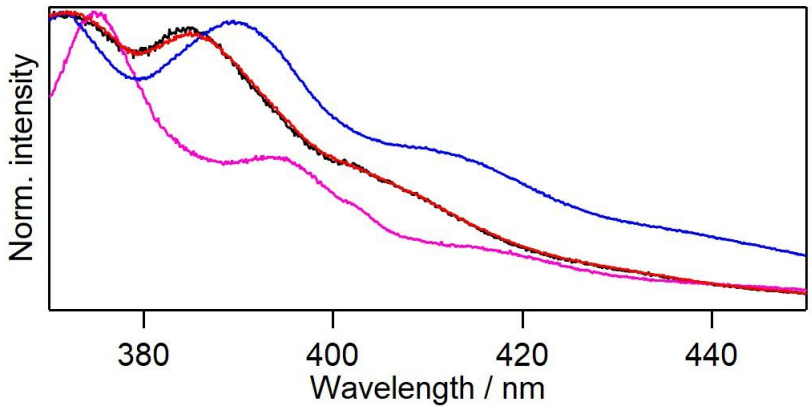

Supplementary Fig. 7 Emission spectra in the range from 370 nm to 450 nm for $[Tb_2(hfa)_6(dptp)_2]$ (black line), $[Nd_2(hfa)_6(dptp)_2]$ (blue line), and dptp ligand (pink line) dissolved in 2-MeTHF (0.1 mM) and Tb-Nd_{MeTHF} (0.1 mM, red line) at 293 K (λ_{ex} = 360 nm). The spectra are normalized at their maximum intensity.

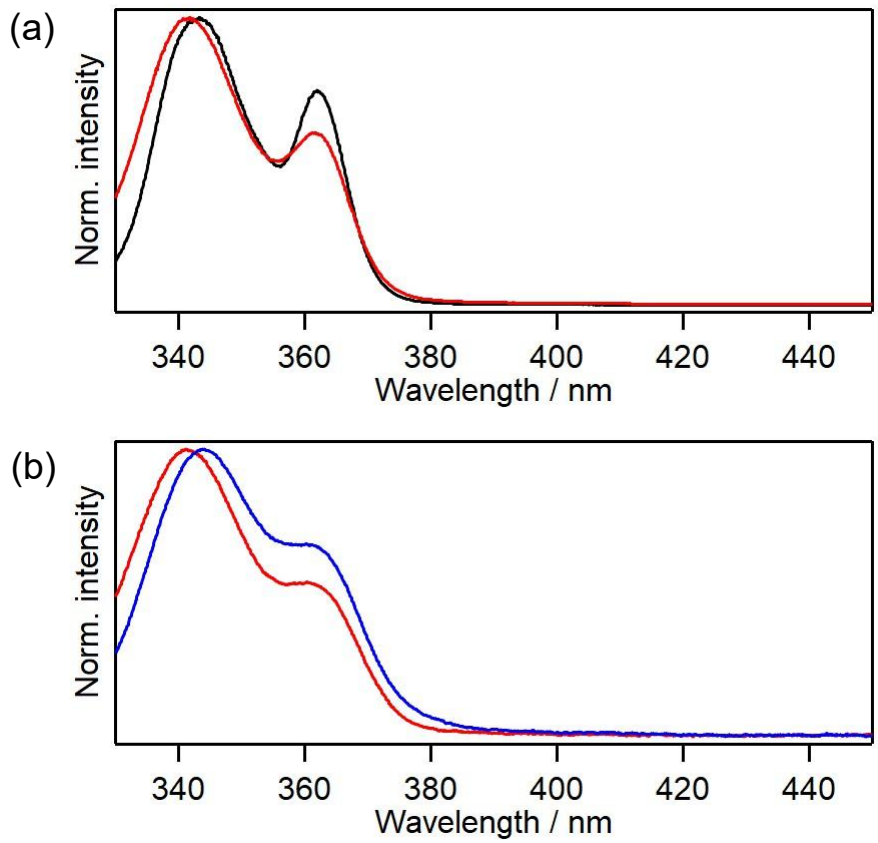

Supplementary Fig. 8 (a) Excitation spectra for Tb(III) emission of $[Tb_2(hfa)_6(dptp)_2]$ (black line) dissolved in 2-MeTHF (0.1 mM) and Tb-Nd_{MeTHF} (0.1 mM, red line) at 293 K (λ_{em} = 542 nm). (b) Excitation spectra for Nd(III) emission of $[Nd_2(hfa)_6(dptp)_2]$ (blue line) dissolved in 2-MeTHF (0.1 mM) and Tb-Nd_{MeTHF} (0.1 mM, red line) at 293 K (λ_{em} = 1060 nm). The spectra are normalized at their maximum intensity.

Supplementary Note 1

Estimation of the rate constant of direct energy transfer from Tb(III) to Nd(III)

The energy transfer rate from Tb(III) to Nd(III) in the direct resonance mechanism can be estimated from the Judd-Ofelt theory[1,2] and its extension to the theory of multipole energy transfer by T. Kushida[3], which was later revisited by O. L. Malta[4]. The energy transfer between lanthanide ions consists of dipole-dipole $W_{\mathrm{ET(dd)}}$, dipole-quadrupole $W_{\mathrm{ET(dq)}}$, quadrupole-dipole $W_{\mathrm{ET(qd)}}$, quadrupole-quadrupole $W_{\mathrm{ET(qq)}}$, and magnetic dipole-dipole $W_{\mathrm{ET(mdmd)}}$ interactions. The rate constants can be calculated from the following equations:

$$W_{\mathrm{ET(dd)}} = \frac{\left(1-\sigma_1^{\mathrm{D}}\right)^2\left(1-\sigma_1^{\mathrm{A}}\right)^2}{(2J_{\mathrm{D}}+1)(2J_{\mathrm{A}}+1)}\frac{2}{3}\frac{4\pi^2}{h}\frac{e^4}{R^6}\left[\sum_{k=2,4,6}\Omega_k^{\mathrm{D}}\left|\langle l^N SLJ\|U^{(k)}\|l^N S'L'J'\rangle\right|^2\right] \times \left[\sum_{k=2,4,6}\Omega_k^{\mathrm{A}}\left|\langle l^N SLJ\|U^{(k)}\|l^N S'L'J'\rangle\right|^2\right]F \quad \text{(S1)}$$

$$W_{\mathrm{ET(dq)}} = \frac{\left(1-\sigma_1^{\mathrm{D}}\right)^2\left(1-\sigma_2^{\mathrm{A}}\right)^2}{(2J_{\mathrm{D}}+1)(2J_{\mathrm{A}}+1)}\frac{4\pi^2}{h}\frac{e^4}{R^8}\left[\sum_{k=2,4,6}\Omega_k^{\mathrm{D}}\left|\langle l^N SLJ\|U^{(k)}\|l^N S'L'J'\rangle\right|^2\right] \times \left[\left|\langle 4\mathrm{f}\|r_{\mathrm{A}}^2\|4\mathrm{f}\rangle\right|^2\left|\langle l\|C^{(2)}\|l\rangle\right|^2\left|\langle l^N SLJ\|U^{(2)}\|l^N S'L'J'\rangle\right|^2\right]F \quad \text{(S2)}$$

$$W_{\mathrm{ET(qd)}} = \frac{\left(1-\sigma_2^{\mathrm{D}}\right)^2\left(1-\sigma_1^{\mathrm{A}}\right)^2}{(2J_{\mathrm{D}}+1)(2J_{\mathrm{A}}+1)}\frac{4\pi^2}{h}\frac{e^4}{R^8}\left[\left|\langle 4\mathrm{f}\|r_{\mathrm{D}}^2\|4\mathrm{f}\rangle\right|^2\left|\langle l\|C^{(2)}\|l\rangle\right|^2\left|\langle l^N SLJ\|U^{(2)}\|l^N S'L'J'\rangle\right|^2\right] \times \left[\sum_{k=2,4,6}\Omega_k^{\mathrm{A}}\left|\langle l^N SLJ\|U^{(k)}\|l^N S'L'J'\rangle\right|^2\right]F \quad \text{(S3)}$$

$$W_{\mathrm{ET(qq)}} = \frac{\left(1-\sigma_2^{\mathrm{D}}\right)^2\left(1-\sigma_2^{\mathrm{A}}\right)^2}{(2J_{\mathrm{D}}+1)(2J_{\mathrm{A}}+1)}\frac{14}{5}\frac{4\pi^2}{h}\frac{e^4}{R^{10}}\left|\langle l\|C^{(2)}\|l\rangle\right|^4\left[\left|\langle 4\mathrm{f}\|r_{\mathrm{D}}^2\|4\mathrm{f}\rangle\right|^2\left|\langle l^N SLJ\|U^{(2)}\|l^N S'L'J'\rangle\right|^2\right] \times \left[\left|\langle 4\mathrm{f}\|r_A^2\|4\mathrm{f}\rangle\right|^2\left|\langle l^N SLJ\|U^{(2)}\|l^N S'L'J'\rangle\right|^2\right]F \quad \text{(S4)}$$

$$W_{\mathrm{ET(mdmd)}} = \frac{\left(1-\sigma_1^{\mathrm{D}}\right)^2\left(1-\sigma_1^{\mathrm{A}}\right)^2}{(2J_{\mathrm{D}}+1)(2J_{\mathrm{A}}+1)}\frac{2}{3}\frac{4\pi^2}{h}\frac{{\mu_{\mathrm{B}}}^4}{R^6}\left[\left|\langle l^N SLJ\|L+gS\|l^N S'L'J'\rangle\right|^2\right] \times \left[\left|\langle l^N SLJ\|L+gS\|l^N S'L'J'\rangle\right|^2\right]F \quad \text{(S5)}$$

where $(1-\sigma_k)$, Ω_k, μ_{B}, R, $\langle l\|C^{(2)}\|l\rangle$, $\langle 4\mathrm{f}\|r^2\|4\mathrm{f}\rangle$, $\langle l^N SLJ\|U^{(2)}\|l^N S'L'J'\rangle$, and $\langle l^N SLJ\|L+gS\|l^N S'L'J'\rangle$ are shielding factor, Judd-Ofelt parameter, Bohr magneton, the distance between the two lanthanide ions, one-electron orientational reduced matrix element, the radial integral, electric-dipole transition reduced matrix elements of tensor operator $U^{(2)}$, and magnetic-dipole transition

reduced matrix elements. The superscript D and A represent the donor and acceptor, which in this case are Tb(III) and Nd(III), respectively. The $\langle l\|C^{(2)}\|l\rangle$ is calculated by the following equation:

$$\langle l\|C^{(2)}\|l\rangle = (-1)^l(2l+1)\begin{pmatrix} l & 2 & l \\ 0 & 0 & 0 \end{pmatrix} \quad \text{(S6)}$$

where $\begin{pmatrix} j_1 & j_2 & j_3 \\ j_4 & j_5 & j_6 \end{pmatrix}$ is Wigner 3-j symbol. The values of $\langle 4f\|r^2\|4f\rangle$ are provided in the literature, and for Tb(III) and Nd(III), the values are 0.893 and 1.222 in squared atomic unit, respectively[5]. The *F* is the spectral overlap integral of the emission and absorption given by the following equation:

$$F = \frac{\ln 2}{\sqrt{\pi}}\frac{1}{\hbar\gamma_D\hbar\gamma_A}\sqrt{\left\{\left(\frac{1}{\hbar\gamma_D}\right)^2+\left(\frac{1}{\hbar\gamma_A}\right)^2\right\}\ln 2}\times\exp\left[\frac{1}{4}\frac{\left(\frac{2\Delta}{\hbar\gamma_D{}^2}\ln 2\right)^2}{\left\{\left(\frac{1}{\hbar\gamma_D}\right)^2+\left(\frac{1}{\hbar\gamma_A}\right)^2\right\}\ln 2}-\left(\frac{\Delta}{\hbar\gamma_D}\right)^2\ln 2\right] \quad \text{(S7)}$$

where $\hbar\gamma_D$, $\hbar\gamma_A$, and Δ are FWHM of emission, FWHM of absorption, and the centroid-to-centroid gap between emission and absorption, respectively. The reduced matrix element $\langle l^N SLJ\|U^{(k)}\|l^N S'L'J'\rangle$ can be calculated based on the following equation:

$$\langle l^N SLJ\|U^{(k)}\|l^N S'L'J'\rangle = (-1)^{S+L'+J+k}\sqrt{(2J+1)(2J'+1)}\begin{Bmatrix} J & J' & k \\ L' & L & S \end{Bmatrix}\langle l^N SL\|U^{(k)}\|l^N SL'\rangle \quad \text{(S8)}$$

$$\langle l^N SL\|U^{(k)}\|l^N SL'\rangle = N\sqrt{(2L+1)(2L'+1)}\sum_{\psi(l^{N-1})}(l^{N-1}\overline{SL}|l^N SL)\begin{Bmatrix} L & l & \bar{L} \\ l & L' & k \end{Bmatrix}(-1)^{\bar{L}+L+l+k} \quad \text{(S9)}$$

Here, $\begin{Bmatrix} j_1 & j_2 & j_3 \\ j_4 & j_5 & j_6 \end{Bmatrix}$ is Wigner 6-j symbol and $\sum_{\psi(l^{N-1})}(l^{N-1}\overline{SL}|l^N SL)$ is the sum of fractional parentage for all of the states of l^{N-1} lanthanide. The reduced matrix element $\langle l^N SLJ\|L+gS\|l^N S'L'J'\rangle$ is given by:

$$\langle l^N SLJ\|L+gS\|l^N S'L'J'\rangle = g\sqrt{J(J+1)(2J+1)} \quad (J'=J) \quad \text{(S10)}$$

$$\langle l^N SLJ\|L+gS\|l^N S'L'J'\rangle = (g-1)\sqrt{\frac{(S+L+J+1)(J+L-S)(J+S-L)(S+L-J+1)}{4J}} \quad (J'=J-1) \quad \text{(S11)}$$

These values for Tb(III) and Nd(III) were calculated on a software Relic 1.0[6].

Although Judd-Ofelt analysis of the complexes are not possible due to lack of enough quantitatively visible absorption band of Tb(III) and Nd(III) ions, the range of rate constant can be estimated based on surveys of the Judd-Ofelt parameters (we will later show that this is an adequate

assessment). We used the database of Judd-Ofelt parameters available online by J. Hrabovsky *et. al.*[7] and took the statistical centroid to obtain the average Judd-Ofelt parameters. The obtained values are provided in Supplementary Table 2.

Supplementary Table 2 Judd-Ofelt parameters for Tb(III) and Nd(III) based on the centroid of the values obtained from the database.

Judd-Ofelt Parameter Ω_λ	Tb(III) / 10^{-20} cm^2	Nd(III) / 10^{-20} cm^2
Ω_2	5.60	2.98
Ω_4	1.69	3.81
Ω_6	2.34	4.52

The shielding factor $(1-\sigma_k)$ can be calculated based on the report by A. N. Carneiro Neto *et. al*[8]. The equation is as follows:

$$(1-\sigma_k) = \rho\left(\frac{2}{1+\rho}\right)^{k+1} \quad \text{(S12)}$$

The overlap integral ρ is given as a parametric function of distance between lanthanide ion and the closest coordinating atom r:

$$\rho(r) = e^{a+br+cr^2} \quad \text{(S13)}$$

Parameter a, b, and c is given by the report and is summarized in Supplementary Table 3 along with the calculated values of ρ and $(1-\sigma_k)$. The distance between the lanthanide ion and the closest coordinating atom was taken from the crystallographic data.

Supplementary Table 3 Shielding factors for Tb(III) and Nd(III).

	r / Å	a	b	c	ρ	$(1-\sigma_1)$	$(1-\sigma_2)$
Nd^{3+}-O^{2-}	2.26	1.095	−2.370	0.172	0.03396	0.1270	0.2458
Tb^{3+}-O^{2-}	2.26	1.417	−1.891	0.078	0.08506	0.2890	0.5327

With these values, the direct energy transfer rate constant from Tb(III) to Nd(III) ion were calculated for various transitions. The values are summarized in Supplementary Table 4.

–

Supplementary Table 4 Energy transfer rate constants from Tb(III) to Nd(III) ion.

Transition		Multipole type				
Tb(III)	Nd(III)	$W_{ET(dd)}$ R^{-6} / cm^6 s^{-1}	$W_{ET(dq)}$ R^{-8} / cm^8 s^{-1}	$W_{ET(qd)}$ R^{-8} / cm^8 s^{-1}	$W_{ET(qq)}$ R^{-10} / cm^{10} s^{-1}	$W_{ET(mdmd)}$ R^{-6} / cm^6 s^{-1}
$^5D_4 \rightarrow {}^7F_6$	$^4I_{9/2} \rightarrow {}^2K_{15/2}$	2.9×10^{-45}	0	8.1×10^{-59}	0	0
$^5D_4 \rightarrow {}^7F_5$	$^4I_{9/2} \rightarrow {}^4G_{7/2}$	1.3×10^{-43}	4.4×10^{-57}	6.2×10^{-57}	1.6×10^{-69}	8.4×10^{-49}
$^5D_4 \rightarrow {}^7F_4$	$^4I_{9/2} \rightarrow {}^2G_{7/2}$	5.3×10^{-44}	2.4×10^{-57}	4.8×10^{-58}	1.6×10^{-70}	3.1×10^{-47}
$^5D_4 \rightarrow {}^7F_4$	$^4I_{9/2} \rightarrow {}^4G_{5/2}$	3.3×10^{-43}	4.1×10^{-56}	3.0×10^{-57}	2.8×10^{-69}	0
$^5D_4 \rightarrow {}^7F_3$	$^4I_{9/2} \rightarrow {}^2H_{11/2}$	3.2×10^{-45}	2.3×10^{-60}	1.8×10^{-58}	7.7×10^{-73}	3.4×10^{-46}
$^5D_4 \rightarrow {}^7F_2$	$^4I_{9/2} \rightarrow {}^2H_{11/2}$	2.8×10^{-45}	1.6×10^{-60}	1.3×10^{-58}	5.6×10^{-73}	0
$^5D_4 \rightarrow {}^7F_2$	$^4I_{9/2} \rightarrow {}^4F_{9/2}$	1.9×10^{-46}	2.9×10^{-61}	8.8×10^{-60}	9.8×10^{-74}	0
$^5D_4 \rightarrow {}^7F_1$	$^4I_{9/2} \rightarrow {}^2H_{11/2}$	2.1×10^{-46}	1.2×10^{-61}	0	0	0
$^5D_4 \rightarrow {}^7F_1$	$^4I_{9/2} \rightarrow {}^4F_{9/2}$	2.6×10^{-45}	3.9×10^{-60}	0	0	0
$^5D_4 \rightarrow {}^7F_0$	$^4I_{9/2} \rightarrow {}^4F_{9/2}$	5.2×10^{-45}	7.8×10^{-60}	0	0	0
Total		5.2×10^{-43}	4.8×10^{-56}	1.0×10^{-56}	4.6×10^{-69}	3.7×10^{-46}

The distance between Tb(III) and Nd(III) ion was found to be 14.6 Å based on the crystallographic data. The total resonance energy transfer rate constant from Tb(III) to Nd(III) was then calculated as $W_{ET} = 1.4$ s^{-1}, which is three orders of magnitude smaller than the decay rate of the $^5D_4$ state of Tb(III) ion (~10^3 s^{-1})[9]. The calculated energy transfer rate constant is based on the average Judd-Ofelt parameters from the database, which means that the actual value may be different in this complex. However, we note that even if all of the Judd-Ofelt parameters were increased by an order of magnitude, the increase in the total rate constant is only about 7 times larger, which is still significantly smaller than the decay rate of the $^5D_4$ state of Tb(III) ion. Therefore, it is safe to assume that the direct energy transfer from Tb(III) to Nd(III) ion in this system is a negligibly small factor.

Supplementary Table 5 Temperature-dependent Tb(III) emission lifetimes (λ_{ex} = 360 nm, λ_{em} = 542 nm) of Tb-Nd_{MeTHF} (0.5 mM) and [$Tb_2(hfa)_6(dptp)_2$] dissolved in 2-MeTHF (0.5 mM).

Temperature / K	Tb-Nd_{MeTHF}		[$Tb_2(hfa)_6(dptp)_2$] / μs
	Short emission lifetime component /μs	Long emission lifetime component /μs	
100	428±2 (58%)	759±1 (42%)	768±4
106.25	418±3 (56%)	755.1±0.3 (44%)	771±4
112.5	419±1 (57%)	758±3 (43%)	770.2±0.3
118.75	409±2 (55%)	748.9±0.2 (45%)	764±1
125	420±5 (60%)	765±6 (40%)	761±4
131.25	403±6 (54%)	741±4 (46%)	758±1
137.5	395.2±0.4 (53%)	739.0±0.2 (47%)	755±1
143.75	387±9 (51%)	734±4 (49%)	754.1±0.1
150	380±1 (50%)	735±5 (50%)	754±1
156.25	368±1 (49%)	727±4 (51%)	751.8±0.5
162.5	353±2 (48%)	719±3 (52%)	747.0±0.3
168.75	341±4 (48%)	713±6 (52%)	741.0±0.1
175	328±3(50%)	707±4 (50%)	734.8±0.4
181.25	315±7 (54%)	703±11 (46%)	728.0±0.2
187.5	295±9 (56%)	695±14 (44%)	719±1
193.75	278±2 (60%)	688±8 (40%)	709±1
200	252±5 (65%)	675±4 (35%)	696.2±0.1
206.3	229±3 (69%)	662±8 (31%)	682.5±0.4
212.5	200±5 (73%)	645±10 (27%)	664±1
218.8	172±4 (76%)	625±11 (24%)	643.7±0.1
225	140±3 (79%)	599±11 (21%)	617±2
231.3	114±2 (80%)	572±11 (20%)	589±2
237.5	90.8±3.3 (81%)	541±14 (19%)	556±4
243.8	70.7±2.8 (82%)	506±15 (18%)	520±1
250	53.7±0.4 (83%)	468±10 (17%)	480±4
256.3	40.5±1.9 (84%)	427±12 (16%)	436±6
262.5	30.8±2.3 (85%)	387±13 (15%)	392±6
268.8	21.8±2.5 (86%)	342±17 (14%)	350±4
275	16.8±0.5 (86%)	299±7 (14%)	304±6
281.3	13.5±1.1 (86%)	261±2 (14%)	259±7
287.5	10.5±1.1 (86%)	217±6 (14%)	219±3
293.8	8.3±0.6 (87%)	183±4 (13%)	180±4
300	6.5±0.4 (87%)	151±1 (13%)	150±4

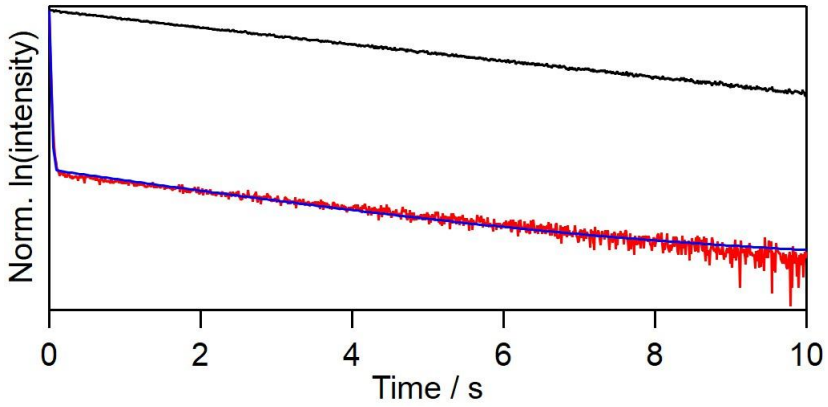

Supplementary Fig. 9 Phosphorescence decay curves of $[Gd_2(hfa)_6(dptp)_2]$ (red line) and dptp (black line) dissolved in 2-MeTHF (0.5 mM) at 80 K (λ_{ex} = 360 nm, λ_{em} = 470 nm,10 ms delay). The decay curve of $[Gd_2(hfa)_6(dptp)_2]$ was fitted by double-exponential function (blue line, τ_1 = 10 ms (99.2%), τ_2 = 2.9 s (0.8%)).

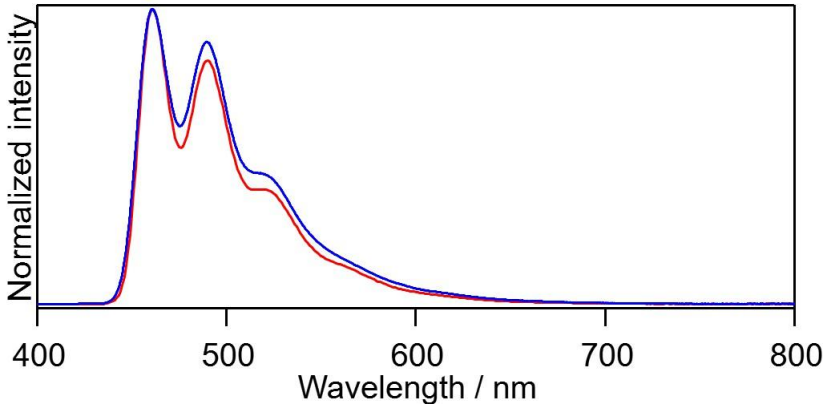

Supplementary Fig. 10 Emission spectra of $[Gd_2(hfa)_6(dptp)_2]$ (red line) and $[Gd(hfa)_3(tppo)_2]$ (blue line) dissolved in 2-MeTHF (0.5 mM) at 80 K (λ_{ex} = 360 nm, 10 ms delay).

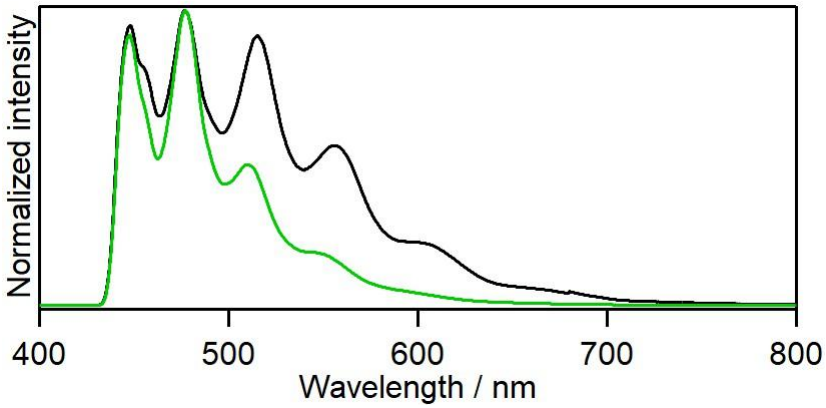

Supplementary Fig. 11 Emission spectra of $[Gd_2(hfa)_6(dptp)_2]$ (black line) and dptp (green line) dissolved in 2-MeTHF (0.5 mM) at 80 K (λ_{ex} = 360 nm, 200 ms delay).

Supplementary Note 2

Additional quenching pathway from Tb(III)

The activation energy corresponding to additional quenching pathway (E_{a2}) of $[Tb_2(hfa)_6(dptp)_2]$ and $[TbNd(hfa)_6(dptp)_2]$ are 6.44×10^2 and 1.96×10^2 cm^{-1}, respectively, which are smaller than the energy difference between the Tb(III) emitting state ($^5D_4$) and the hfa triplet state (1,200 cm^{-1}) and between the $^5D_4$ state and the dptp triplet state (2,000 cm^{-1}). Therefore, the additional quenching pathway may originate from the energy transfer from the $^5D_4$ state (Tb(III)) to the dark states such as ligand-to-ligand charge transfer states[10].

Supplementary Table 6 Tb(III) emission lifetimes of $[Tb_2(hfa)_6(dptp)_2]$ dissolved in 2-MeTHF (0.5 mM) and Tb-Nd_{MeTHF} (0.5 mM) under N_2, air, and O_2 atmosphere.

Condition	[a]$[Tb_2(hfa)_6(dptp)_2]$ / μs	[a]Tb-Nd_{MeTHF} / μs
N_2	141	7.1 (80%), 134 (20%)
Air	82	6.9(80%), 79 (20%)
O_2	28	6.2 (76%), 27 (24%)

[a]293 K, λ_{ex} = 360 nm, λ_{em} = 542 nm.

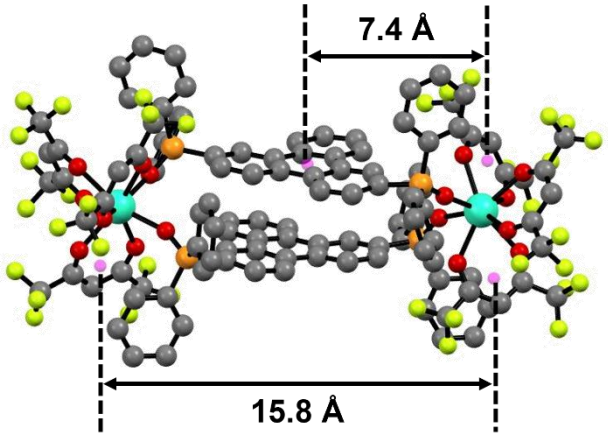

Supplementary Fig. 12 The shortest distances between hfa_{Tb}-dptp and hfa_{Tb}-hfa_{Nd} centroids (purple spheres) in the single-crystal structure of $[Tb_2(hfa)_6(dptp)_2]$. Carbon, oxygen, fluorine, phosphorus, and terbium atoms are represented by gray, red, light green, orange, and green spheres, respectively. Hydrogen atoms are omitted for clarity.

Supplementary Note 3

Analyses of Nd(III) emission lifetime

To verify that the insertion of Nd(III) ion shortens the triplet state lifetime of hfa_{Tb}, we estimated the Nd(III) emission lifetime in $[Nd_2(hfa)_6(dptp)_2]$ (2-MeTHF, 0.5 mM) and Tb-Nd_{MeTHF} (0.5 mM). Time-resolved emission analyses at 300 K revealed a double-exponential decay for Nd(III) emission in Tb-Nd_{MeTHF} (Supplementary Fig 13). The Nd(III) emission lifetimes of Tb-Nd_{MeTHF} were estimated to be 2.1 μs (96%) and 7.3 μs (4%) (Supplementary Table 7). The shorter emission lifetime component was similar to the emission lifetime of $[Nd_2(hfa)_6(dptp)_2]$ (1.5 μs), which are attributed to the Nd(III) emission upon energy transfer from ligands to Nd(III). The longer emission lifetime component can be assigned to the delayed Nd(III) emission *via* ligand-assisted energy transfer from Tb(III) to Nd(III) in $[TbNd(hfa)_6(dptp)_2]$. The delayed Nd(III) emission lifetime (7.3 μs) was comparable with the Tb(III) emission lifetime in $[TbNd(hfa)_6(dptp)_2]$ (6.5 μs). This situation also occurred in the temperature range of 200-300 K (Supplementary Fig. 14). Thus, the ligand-assisted energy transfer from Tb(III) to Nd(III) occurs in $[TbNd(hfa)_6(dptp)_2]$.

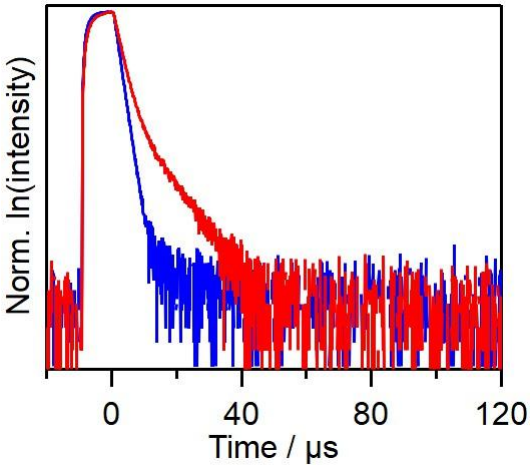

Supplementary Fig. 13 Nd(III) emission decay curves of $[Nd_2(hfa)_6(dptp)_2]$ (blue) dissolved in 2-MeTHF (0.5 mM) and Tb-Nd_{MeTHF} (red, 0.5 mM) at 300 K (λ_{ex} = 360 nm, λ_{em} = 1053 nm). The emission decay curves are normalized at their maximum intensity.

Supplementary Table 7 Temperature-dependent Nd(III) emission lifetimes of Tb-Nd_{MeTHF} (0.5 mM, λ_{ex} = 360 nm, λ_{em} =1053 nm).

Temperature / K	Short emission lifetime component /μs	Long emission lifetime component /μs
100	1.6 (99.994%)	371 (0.006%)
112.5	1.6 (99.994%)	376 (0.006%)
125	1.6 (99.994%)	358 (0.006%)
137.5	1.6 (99.994%)	338 (0.006%)
150	1.6 (99.994%)	347 (0.006%)
162.5	1.6 (99.993%)	314 (0.007%)
175	1.6 (99.99%)	296 (0.01%)
187.5	1.7 (99.99%)	271 (0.01%)
200	1.7 (99.97%)	237 (0.03%)
[a]212.5	2.3 (90%)	193 (10%)
[a]225	2.1 (95%)	135 (5%)
237.5	2.0 (99.8%)	85 (0.2%)
250	2.1 (99.7%)	53 (0.3%)
262.5	2.1 (99.4%)	31 (0.6%)
275	2.1 (99%)	19 (1%)
287.5	2.1 (98%)	11 (2%)
300	2.1 (96%)	7.3 (4%)

[a]Estimated by double-exponential tail fitting.

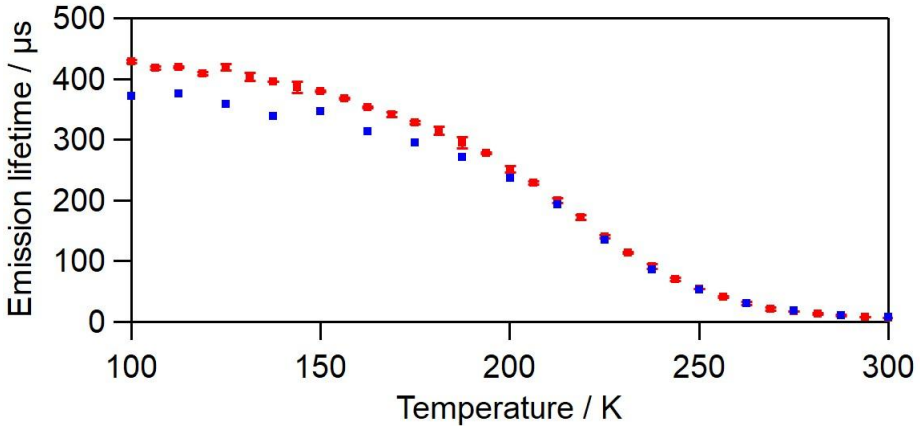

Supplementary Fig. 14 Temperature-dependent Tb(III) emission lifetimes (λ_{ex} = 360 nm, λ_{em} = 542 nm, red dots) and the delayed Nd(III) emission lifetimes (λ_{ex} = 360 nm, λ_{em} = 1053 nm, blue dots) of [TbNd(hfa)$_6$(dptp)$_2$] dissolved in 2-MeTHF. Error bar represents standard deviation.

Supplementary References

1. Judd, B. R. Optical absorption intensities of rare-earth ions. *Phys. Rev.* **127**, 750–761 (1962).
2. Ofelt, G. S. Intensities of crystal spectra of rare-earth ions. *J. Chem. Phys.* **37**, 511–520 (1962).
3. Kushida, T. Energy transfer and cooperative optical transitions in rare-earth doped inorganic materials. I. transition probability calculation. *J. Phys. Soc. Jpn.* **34**, 1318–1326 (1973).
4. Carneiro Neto, A. N. *et al.* Theoretical and experimental investigation of the $Tb^{3+} \rightarrow Eu^{3+}$ energy transfer mechanisms in cubic $A_3Tb_{0.90}Eu_{0.10}(PO_4)_3$ (A = Sr, Ba) materials. *J. Phys. Chem. C* **124**, 10105–10116 (2020).
5. Edvardsson, S. & Klintenberg, M. Role of the electrostatic model in calculating rare-earth crystal-field parameters. *J. Alloy Comp.* **275–277**, 230–233 (1998).
6. Hehlen, M. P., Brik & M. G., Krämer, 50^{th} anniversary of the judd-ofelt theory: an experimentalist's view of the formalism and its application. *J. Lumin.* **136**, 221–239 (2013).
7. Hrabovsky, J., Krystufek, R. & Varak, *Judd-Ofelt Database*, LOMS. https://www.loms.cz/
8. Carneiro Neto, A. N. & Moura, R. T. Jr. Overlap integrals and excitation energies calculations in trivalent lanthanides 4f orbitals in paris Ln-L (L = Ln, N, O, F, P, S, Cl, Se, Br, and I). *Chem. Phys. Lett.* **757**, 137884 (2020).
9. Inage, K., Wang, M., Hasegawa, Y. & Kitagawa, Y. Effective photosensitized emission of a Tb(III) complex using a β-diketonate photosensitizer and an oxygen barrier system in a thermally populated triplet state. *Dalton Trans.* **53**, 8555–8562 (2024).
10. Ferreira da Rosa, P. P. *et al.* Thermosensitive seven-coordinate Tb^{III} complexes with LLCT transitions. *Eur. J. Inorg. Chem.* **2018**, 2031–2037 (2018).